nature communications

Article

https://doi.org/10.1038/s41467-025-61715-z

High-temperature quantum coherence of spinons in a rare-earth spin chain

Received: 25 October 2024

Accepted: 26 June 2025

Published online: 17 July 2025

Check for updates

Lazar L. Kish[1], Andreas Weichselbaum[1], Daniel M. Pajerowski[2], Andrei T. Savici[2], Andrey Podlesnyak[2], Leonid Vasylechko[3], Alexei Tsvelik[1], Robert Konik[1] & Igor A. Zaliznyak[1]

Conventional wisdom dictates that quantum effects become unimportant at high temperatures. In magnets, when the thermal energy exceeds interactions between atomic magnetic moments, the moments are usually uncorrelated, and classical paramagnetic behavior is observed. This thermal decoherence of quantum spin behaviors is a major hindrance to quantum information applications of spin systems. Remarkably, our neutron scattering experiments on Yb chains in an insulating perovskite crystal defy these conventional expectations. We find a sharply defined spectrum of spinons, fractional quantum excitations of spin-1/2 chains, to persist to temperatures much higher than the scale of the interactions between Yb magnetic moments. The observed sharpness of the spinon continuum's dispersive upper boundary indicates a spinon mean free path exceeding ≈ 35 inter-atomic spacings at temperatures more than an order of magnitude above the interaction energy scale. We thus discover an important and highly unique quantum behavior, which expands the realm of quantumness to high temperatures where entropy-governed classical behaviors were previously believed to dominate. Our results have profound implications for spin systems in quantum information applications operating at finite temperatures and motivate new developments in quantum metrology.

Magnetism is the oldest quantum phenomenon, known for nearly 2500 years before it was understood following the discovery of electron spin[1] and the invention of quantum mechanics[2]. Beyond simple ferromagnetism, quantum theory predicts a great variety of other collective spin states, such as in exactly solved antiferromagnetic spin-1/2 chains[3,4], where spins exhibit long-range quantum entanglement but no static magnetic order. Consequently, spin systems are widely considered for quantum information applications requiring quantum-coherent processing, transmission, and storage of entangled states. Quantum computation and communication algorithms using spin chains[5–9], fractional and topological excitations in quantum spin liquids[10–12], as well as magnons in ordered ferro- and antiferromagnets[13–15] are currently being investigated.

The magnetic doublets of rare earth Kramers ions such as Yb^{3+} in a crystal electric field (CEF) provide a fruitful approach to implementing quantum spin qubits in solids[16–19]. Although such a doublet has orbital character imposed by a strong spin-orbit coupling (SOC), it can be represented as a pseudo-spin-1/2, similar to the real spin-1/2 of an unpaired magnetic electron, implementing a quantum qubit. Advantageously, the states of a doublet can carry large angular momentum quantum numbers, which suppresses their interaction with magnetic fields of the environment by virtue of selection rules expressing angular momentum conservation[2]. Hence, rare earth spin qubits can have longer coherence times[17,18]. Such is the situation of Yb^{3+} ions in $YbAlO_3$[20–23], which we study here. Strong SOC (one of the strongest among all lanthanides) combines the spin ($S = 1/2$) and the orbital

[1]Condensed Matter Physics and Materials Science Division, Brookhaven National Laboratory, Upton NY 11973, USA. [2]Neutron Scattering Division, Oak Ridge National Laboratory, Oak Ridge TN 37831, USA. [3]Lviv Polytechnic National University, Lviv, Ukraine. e-mail: zaliznyak@bnl.gov

($L = 3$) angular momenta of a single hole in the 4*f* shell of Yb^{3+} into a total angular momentum $\boldsymbol{J}$ ($J = 7/2$) state, effectively quenching the spin degree of freedom by rigidly tying it to the dominant orbital contribution. This leads to a very simple electronic level structure, which is within the reach of near-infrared or visible photons. Consequently, Yb atoms make the world's most accurate atomic clocks, highly efficient high-power crystal and fiber lasers and optical amplifiers, and are a promising system for optically controlled quantum information applications[17]. A chain of coupled Yb spins (doublets) in $YbAlO_3$ implements a chain of coupled spin qubits where coherently propagating spinon excitations act to switch the state of each qubit, as illustrated in Fig. 1A1.

The main hurdle for quantum computing applications is a decoherence of entangled states when unwanted interactions with the environment or thermal excitations cause quantum information to be lost. The long-range coherence of quantum states existing at zero temperature, $T = 0$, can be destroyed at $T > 0$ when excitations change their identities by colliding and exchanging quantum numbers, as is seen in the thermal decoherence of phonon-roton excitations in superfluid helium[24]. In a quantum spin-1 chain, where the Haldane ground state is disordered, magnon excitations are separated from it by an energy gap, Δ_H, and exhibit mesoscopic long-range coherence at $T = 0$[25]. However, coherence is rapidly lost as magnons become thermally excited at temperatures $k_BT \sim \Delta_H$ (k_B is Boltzmann constant)[25–27]. Such decoherence of the magnon excitations which encode quantum states can be described as a finite collisional lifetime, which in this case can be accurately calculated[28]. A similar phenomenology can be seen in ordered magnets as well, where magnons become over-damped, entirely losing their coherent quantum nature as the thermal energy becomes comparable to magnon bandwidths[29,30]. This thermal decoherence limits the potential applications of magnons for the storage and transmission of quantum information.

Here, we find an entirely different situation in the case of spinons, fractional excitations in a spin-1/2 chain. Our magnetic inelastic neutron scattering (INS) measurements show that in a material realization of spin-1/2 chains in the rare earth perovskite $YbAlO_3$[20–22] spinons retain their quantum coherence to temperatures where thermal energy exceeds characteristic energy scales of spin interactions by more than an order of magnitude. Moreover, an eventual reduction of quantum coherence at our highest measured temperatures stems from interactions with high-energy thermal bath-type degrees of freedom external to the effective spin Hamiltonian.

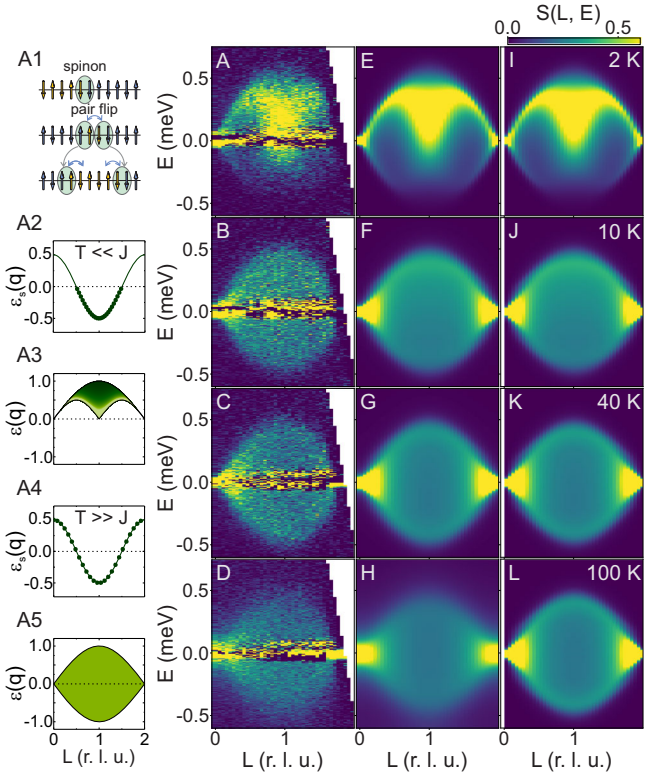

Fig. 1 | The spinon spectra in $YbAlO_3$ at different temperatures. A1 Schematic illustration of spinons as topological defects in antiferromagnetic spin chain; spinon pairs measured in our INS experiments are created by pairwise nearest-spin flips. **A2**–**A5** schematics of how half-filled fermion band gives rise to two-spinon continuum boundaries (see also Supplementary Information). **A**–**D** Color contour maps of the spectral density of the measured neutron scattering intensity at different temperatures: 2 K, 10 K, 40 K, 100 K, top to bottom. These data are integrated in the dispersionless transverse directions with $K = [-1.0, 1.0]$ and $H = [-0.25, 0.25]$. **E**–**H** Fits to model constructed from DMRG calculations with Lorentzian broadening accounting for spinon lifetime, as reported in the main text, directly comparable to neutron data. **I**–**L** Resolution-corrected DMRG calculations without additional Lorentzian broadening accounting for spinon finite lifetime for comparison.

Results

Connecting theory and experiment

While spin-1/2 chains in magnetic crystals have been studied in the past[31–34], to our knowledge the important question of what happens to spinon excitations at temperatures high compared to the exchange coupling energy scale remains experimentally unexplored. This is largely because the exchange energy scales in most studied spin-chain materials are in the range of tens to hundreds of meV ($J/k_B \sim 100 - 1000$ K, k_B is Boltzmann constant), making it difficult to access temperatures truly in excess of the interaction energies—for example, in $KCuF_3$, $J/k_B \approx 400$ K, well above room temperature[33]. From this perspective, $YbAlO_3$ is an ideal material to study because of the relatively weak exchange interaction in its effective spin-1/2 Hamiltonian ($J \approx 0.21$ meV, $J/k_B \approx 2.4$ K[21,22]) and the absence of magnetic order down to a temperature of 0.8 K. As a result, we can use inelastic neutron spectroscopy to probe the physics of the Heisenberg spin-1/2 chain in a temperature regime that is unattainable in other spin-1/2 chain materials.

The spin-1/2 Heisenberg Hamiltonian is a well-established low-energy effective description of a Mott-insulating Hubbard chain at half-filling[35–38]. In $YbAlO_3$, a transparent insulator with an optical gap of approximately 5 eV, the Yb^{3+} ions form chains characterized by an estimated Hubbard interaction $U \sim 20$ eV and hopping amplitude $t \sim 50$ meV[35,39]. These parameters yield an exchange coupling $J \sim 4t^2/U \sim 0.5$ meV, which is roughly consistent with experiment and supports the validity of the low-energy spin-1/2 model[38]. The temperature range explored in this work lies well below the regime[37] where the charge sector above the Mott gap becomes relevant. The effective spin-1/2 Hamiltonian, accounting for the large orbital degeneracy of the Yb $J = 7/2$ multiplet in this parameter range, was rigorously derived from the one-dimensional Hubbard model in ref. 36. The crystal-field splitting between the ground and first excited doublets of the Yb multiplet, estimated to be ~20–30 meV[21], thus represents the lowest atomic energy scale that can compromise the spin-1/2 description at elevated temperatures.

Here, we report a detailed INS investigation of the spinon spectrum in $YbAlO_3$ as a function of temperature in the 2 – 100 K (~(1 – 40) × J) range. The excitation spectrum of the ideal spin-1/2 Heisenberg chain is known to consist of pairs of spinons, fractional elementary excitations each carrying S = 1/2 angular momentum[3,4]. Pair-states of these spinon excitations encode physical spin flips in the chain [this is schematically illustrated in Fig. 1(A1)], whose energy spectrum forms a continuum, at zero-temperature sharply bounded by the two-spinon boundaries (q is the wave vector, d is the lattice

spacing)[31–34,40],

$$\frac{\pi}{2}J|\sin qd| \le \epsilon(q) \le \pi J|\sin\left(\frac{qd}{2}\right)| \quad (1)$$

Qualitatively, the lower and upper two-spinon continuum boundaries show different behavior as a function of temperature, which can be understood by considering spinons as fermion quasiparticles half-filling the one-dimensional energy band, $\epsilon_s(q) = \frac{\pi}{2}J \sin qd$[23,41] (See Supplementary Information for details of data and theoretical analysis and DMRG calculations.). The lower continuum boundary arises because of the complete occupation of states below the spinon Fermi energy at zero temperature, which forbids excitations into the filled states [Fig. 1(A2,A3)]. With the increasing temperature, the Fermi distribution smears out, allowing state occupations above the Fermi level at the expense of the occupied states below it [Fig. 1(A4)]. As a result, the lower boundary blurs until it completely disappears at temperatures $\gtrsim \frac{\pi}{2}J/k_B$. On the other hand, the upper boundary reflects the maximum energy that a spinon pair with a given q can have according to the dispersion, $\epsilon_s(q)$. In the absence of spinon decoherence through a finite collisional lifetime in the idealized system described by the quantum spin-chain Hamiltonian, the profile of the upper two-spinon boundary must remain completely untouched by temperature effects [Fig. 1(A5)]. The upper boundary of the excitation continuum is only blurred beyond the two-spinon boundary by the presence of multi-spinon-excitations. At $T = 0$, the total spectral weight above this upper boundary from such excitations is relatively small (~1%)[40]. While this blurring is in fact temperature-dependent, it is entirely governed by the quantum spin Hamiltonian and as our theoretical calculations show remains insignificant even at high temperatures, $T \gg J/k_B$.

Effects of finite lifetime on spinon spectra

In the presence of couplings to a system external to the quantum spin Hamiltonian, such as a thermal heat bath or other extrinsic source of decoherence, a quantum spin-chain will experience information loss to these external degrees of freedom. This will be reflected by a reduced spinon lifetime, measurable in neutron spectra by a broadening along the energy direction beyond instrument resolution. A blurring of the upper boundary of the excitation continuum in excess of the theoretically calculated width generated by multi-spinon excitations is then a metric for spinon decoherence, quantifying the degree of information loss from the spin-chain to the environment.

Theoretically, the sharp upper boundary of the two-spinon continuum in the dynamical structure factor, as measured by inelastic neutron scattering, is determined by the step-like behavior arising from the integration of a delta function that enforces energy conservation over the internal momentum of the two-spinon states[40,42–47]. Equivalently, this corresponds to integrating single-particle Green's functions within the two-particle susceptibility (see the discussion in Supplementary Information Section II E for the case of the Jordan-Wigner fermion representation). When spinon eigenstates acquire a finite lifetime τ, the delta function transforms into a Lorentzian profile with half-width $\Gamma = \hbar/\tau$. This transformation is mathematically represented as a convolution of the original expression with a Lorentzian function of half-width Γ. Assuming that the lifetime τ is wave-vector independent—an assumption justified *a posteriori* by comparison with experiment—this convolution can be moved outside the integration over the internal momentum of the spinon pair and applied directly to the dynamical structure factor of an ideal chain, thereby modifying the previously calculated sharp two-spinon boundary to reflect finite-lifetime effects.

While our treatment of the finite lifetime of unbound two-spinon states is phenomenological, a comparison with the experimental results presented below demonstrates that it adequately captures the essential physics of spinon decoherence. The analysis shows that decoherence arises from the thermal activation of a crystal-field doublet whose energy is approximately two orders of magnitude larger than that of the spinon dispersion, providing strong physical justification for neglecting the wave-vector dependence of the lifetime. Finally, we note that in extracting the finite spinon lifetime, we rely on comparison with state-of-the-art DMRG calculations, which are widely recognized as one of the most accurate numerical methods for one-dimensional quantum spin systems, particularly the spin-1/2 Heisenberg chain, where it has been extensively benchmarked against exact solutions from the Bethe ansatz[48,49].

Analysis of spinon spectra with finite lifetime

Figure 1 shows the temperature dependence of the measured spinon continuum in $YbAlO_3$ side-by-side with temperature-dependent realizations of the spin-1/2 Heisenberg model from finite-temperature DMRG calculations (see "Methods"). The left column shows our experimentally measured dynamical structure factors, normalized to absolute units as described in the Supplementary Information. The middle column shows a fit of our DMRG-calculated spectra to the experimental data, including convolution with the known instrumental resolution function and a Lorentzian broadening function with half-width Γ to model finite spinon life-time, $\tau = \hbar/\Gamma$[24,26]. The right column shows the DMRG calculations without the Lorentzian broadening, demonstrating how the spectrum would appear if the effects of spinon thermal decoherence were absent. The waterfall plot in Fig. 2 shows constant-L line-cuts of data and the corresponding Lorentzian-broadened DMRG calculation at selected wave-vectors, which demonstrates the excellent agreement between our model and data (values for the reduced χ^2 goodness-of-fit parameter are listed in the caption and are below 3 for all temperatures; L is the component of the wave vector, $Q = (H, K, L)$, along the chain direction, see "Methods").

At 2 K, the lower continuum boundary is visible in both experiment and DMRG simulations, albeit already slightly blurred by thermal repopulation as temperature is comparable to the exchange coupling, $J/k_B = 2.4$ K. At higher temperatures, 10 K and above, all signs of the lower continuum boundary have disappeared in both experiment and simulation [Fig. 1A–D] and instead been replaced by a flat continuum [Fig. 2B–D]. This flat continuum, however, remains clearly bounded by the dispersive upper boundary even at temperatures far higher than the exchange coupling. Remarkably, our experimentally measured datasets demonstrate this clear upper-boundary dispersion at temperatures as high as 100 K, forty times greater than the exchange interactions within the system. Only a slight blurring of the upper boundary can be seen, which is most clearly visible in the 1-dimensional plots in Fig. 2. This blurring appears well modeled by the wave-vector-independent Lorentzian damping, Γ, indicating finite spinon lifetime at high temperatures.

Figure 3A shows Γ as a function of temperature, revealing no measurable spectral broadening beyond resolution at temperatures below 60 K. Above this point, however, the dispersion does become measurably blurred, with Γ eventually reaching an energy-scale of ~0.1 meV at 100 K, consistent with thermally activated behavior. An Arrhenius type fit, $\Gamma(T) = \Gamma_0 e^{-\frac{E_a}{k_B T}}$, yields activation energy of $E_a \approx 20$ meV. This energy scale is consistent with the thermal population of crystal-field levels other than the ground-state doublet, which invalidates the $S_{\text{eff}} = 1/2$ description of the Yb ions, leading to decoherence and information loss. Slight thermal depletion of the ground-state doublet is also consistent with a subtle reduction in the integrated intensity of the measured spinon continuum above 60 K, visible in the inset of Fig. 3A, though this effect is small (with $\lesssim 10\%$ of doublets thermally activated at 100 K) and lies at the limit of our experimental accuracy. The onset of this decoherence mechanism would shift to higher temperatures if the first excited crystal-field level

https://doi.org/10.1038/s41467-025-61715-z

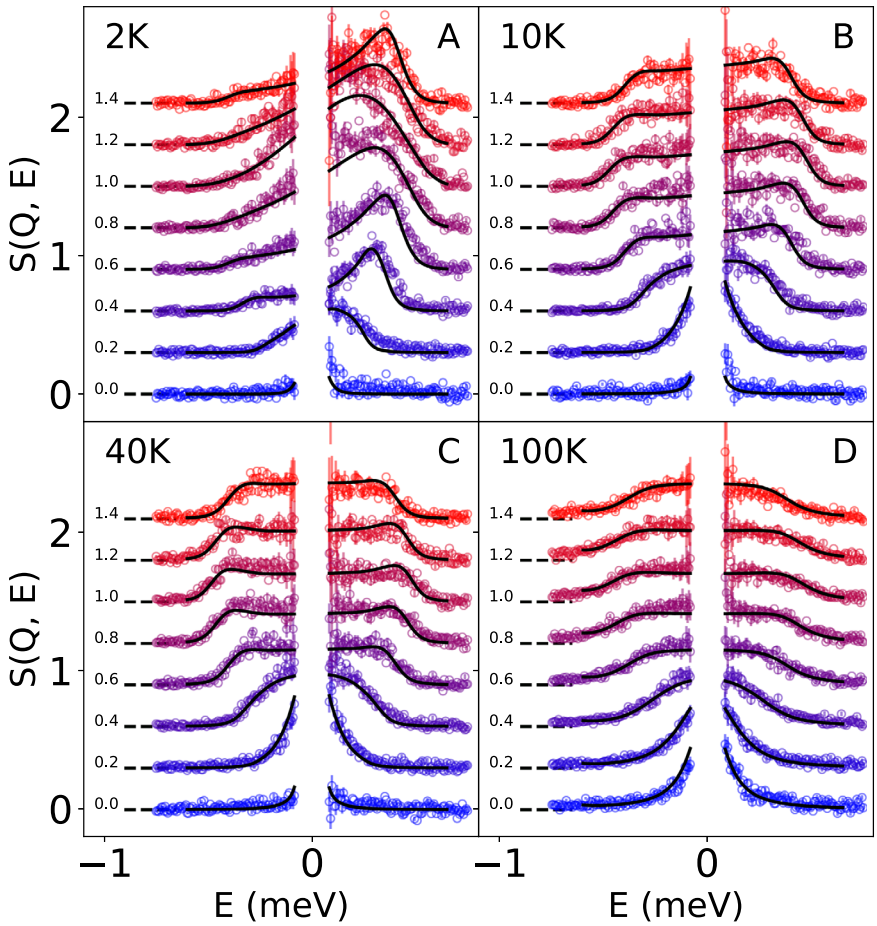

Fig. 2 | Line cuts along the energy axis of our data and fits to our model. Curves are given an incremental offset for visualization, with dashed leader-lines from each curve signifying the zero of intensity. The labels next to each curve signify the central L value of each line-cut, which are 0.2 r. l. u. wide. **A** 2 K (r. $\chi^2 = 2.1$). **B** 10 K (r. $\chi^2 = 1.9$). **C** 40 K (r. $\chi^2 = 1.3$). **D** 100 K (r. $\chi^2 = 1.2$). Error bars represent one standard deviation (SD).

were higher in energy and would vanish entirely if its energy were infinite.

We note that according to the Bethe ansatz, spinons are coherent quasiparticles in the 1D spin-1/2 Heisenberg chain with a well-defined dispersion $\epsilon(q) = \frac{\pi}{2} J \sin q$[40,42–47], which is experimentally revealed through the sharp boundaries of the two-spinon continuum. In our estimate of the coherence length, we use the maximum group velocity derived from this dispersion, which reflects the maximum physical propagation speed of a single spinon excitation. As pointed out by Scheie et al. in ref. 49 and highlighted in Fig. 4 of our manuscript, this velocity is also experimentally revealed through a "light cone" feature in the Fourier-transformed real space-time response function, reflecting the maximum excitation propagation speed in the system, which is directly measurable from neutron scattering data. The coherence length, $\xi \sim v\tau$, thus represents the distance over which a spinon can propagate coherently in the presence of finite-lifetime effects.

Using the group velocity of spinons from the dispersion near $L = 0$, $v = \pi J/2$, we can obtain an effective spinon coherence length (mean free path), $\xi = v\tau = v\hbar/\Gamma$, shown in Fig. 3B versus the reciprocal of temperature. When measurable broadening does develop at temperatures above 60 K, the effective coherence length appears to track a decreasing exponential trend with increasing temperature. Fits to an Arrhenius-type model, $\xi = \xi_0 e^{\frac{E_a}{k_B T}}$, where values $\xi > \xi_0$ are replaced by a fitted constant $\xi_0 \approx 35$ in agreement with our resolution limit, are shown over-plotted on the measured data in Fig. 3B. According to this analysis, the coherence length exceeds 35 lattice units as it passes beyond the resolution limit of our measurements at staggeringly high temperature of 40 K ($\approx 17J$). The value of $E_a \approx 20$ meV obtained through this analysis is close to values for the CEF splitting reported in the literature[21]. Thus, the major spin-decoherence mechanism at play is likely to be thermal excitation of crystal-field levels outside the $S_{\text{eff}} = 1/2$ doublet, which presents defects in the chain that are able to change the number of spinons in the system on measurable timescales.

The coherence length encoded in the spinon lifetime exceeds ≈ 35 lattice units ($\xi > 12$ nm) and is comparable to the mesoscopic quantum coherence length of Haldane-gap magnons observed near zero temperature in spin-1 chains[25]. There, however, magnon coherence is quickly lost with the increasing temperature due to collisions that change the quasiparticle content of the excited states and therefore limit the quasiparticle lifetime[25,27,28]. Consequently, magnons become over-damped at temperatures where thermal energy becomes comparable to the energy of spin interactions. Remarkably, this collisional lifetime mechanism is absent in the case of spinons in the spin-1/2 chain as spinons retain their intrinsic coherence at temperatures much higher than those characteristic of the spin Hamiltonian.

Quantum Fisher information in the high-temperature limit

It is of interest to put our results in the context of quantum metrology, which allows calculating model-independent quantities called entanglement witnesses that can be used to place bounds on the degrees of multipartite quantum entanglement present in the system[50,51]. Of

https://doi.org/10.1038/s41467-025-61715-z

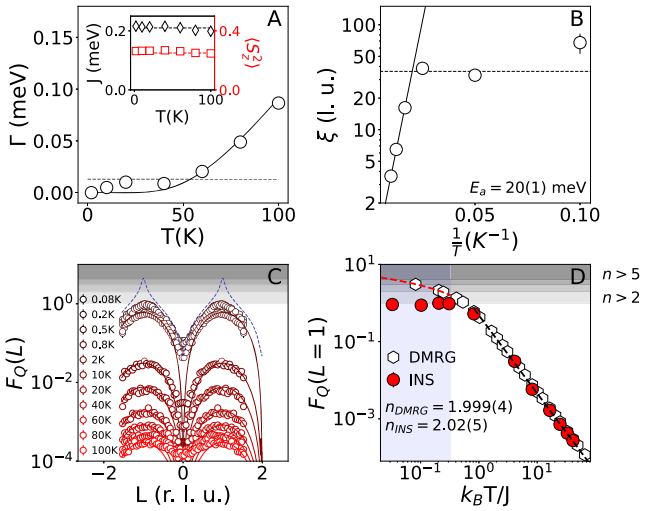

Fig. 3 | Temperature dependence of INS spectral parameters and quantum Fisher information (F_Q). **A** Life-time broadening parameter as a function of temperature. Dashed line is instrumental resolution HWHM (= 0.013 meV) calculated for $E = 0.5$ meV. Solid curve is a fit to Arrhenius-type exponential function as described in the text. The inset shows fitted exchange interaction, J, and integrated intensity, $\langle S_z^2 \rangle$, at different temperatures; horizontal lines indicate nominal values, $J = 0.21$ meV[21,22] and $\langle S_z^2 \rangle = 1/4$. **B** Coherence length calculated using the spinon dispersion and extracted lifetime. Solid and dashed lines are asymptotic Arrhenius and resolution-limited behaviors as in (**A**). **C** Wave-vector dependence of the QFI, $F_Q(L)$, at various temperatures. Dashed curve is an approximation to asymptotic zero-temperature limit calculated from DMRG data at 200 mK as described in the text. **D** Temperature dependence of maximal quantum Fisher information, $F_Q(L = 1)$. Dashed black line is a power-law fit to the data in $T \geq 2$ K range capturing asymptotic high-temperature behavior, $F_Q \sim (J/T)^n$, with $n = 2$. Dashed red curve, shown in the region below $T_N = 0.8$ K (shaded), is a fit of DMRG data below 4 K to a logarithmic dependence, $F_Q = [\ln(aJ/k_BT)]^\alpha$, with $J = 0.21$ meV and fitting parameters $a = 1.55(2)$ and $\alpha = 1.04(1)$, illustrating the low-T asymptotic behavior; in $YbAlO_3$ it is arrested by static order below T_N, where part of the excitation spectrum condenses into elastic Bragg peaks that do not contribute to QFI. Error bars represent one SD and, where not visible, are smaller than the symbol size.

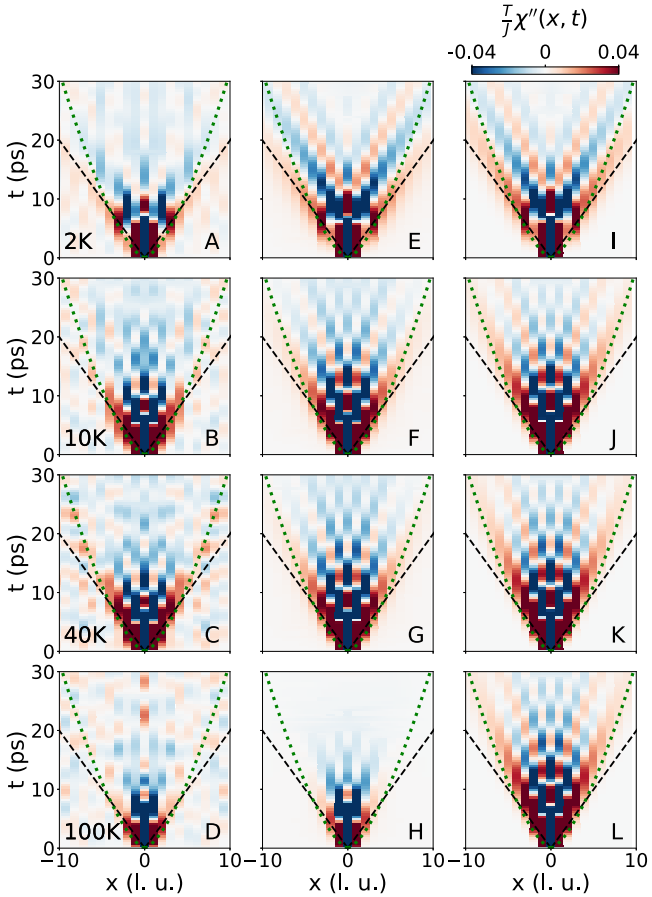

Fig. 4 | Direct-space and time response functions, $\chi''(x, t) = -\mathbf{i}F[\chi''(Q, E)]$, as a function of temperature. **A**–**D** Calculated from inelastic neutron scattering spectra; **E**–**H** Calculated from fits to inelastic neutron data; **I**–**L** Obtained from DMRG calculations. Dashed black lines mark the edge of the light-cone in the ballistic regime, $t = \frac{x}{2\pi v}$, while dotted green curves highlight the long-time super-diffusive behavior, $t \sim x^{3/2}$ [54], prominent at high temperatures.

specific relevance is the quantum Fisher information (QFI), $F_Q(\hat{A})$[52], a quantity that can be defined at finite temperature for any system through an imaginary part of dynamical susceptibility with respect to a variable, $\hat{A}$, in that system, $\chi''_A(E)$,

$$F_Q(\hat{A}) = \frac{1}{4\pi}\int_0^\infty dE \tanh\left(\frac{E}{2k_BT}\right)\chi''_A(E) \quad (2)$$

For the spin-1/2 chain, the QFI, F_Q, can be obtained for $\hat{A} = \hat{S}^z$ from the dynamical spin susceptibility at any wave-vector, $\chi''(Q, E)$. Equivalently, it can obtained from the dynamical spin structure factor, $S(Q, E)$, measured by INS (Fig. 1), which is related to $\chi''(Q, E)$ via the fluctuation-dissipation theorem[26,50,51]. The obtained QFI can then be used to place lower limits on the level of multipartite entanglement in the system, where QFI $F_Q > n$ at a certain wave vector imply at least $(n+1)$-partite entanglement in the system (Kramers-Rao bound)[50–52] provided no symmetries are taken into account.

Figure 3C shows the wave-vector-dependent QFI calculated from our neutron spectra for temperatures down to 80 mK (open circles), as well as from our idealized DMRG model (solid curves). The dashed curve represents an approximation to the theoretical maximum at zero temperature, $F_Q|_{T=0} = 4S(Q)$[49], where $S(Q) = \int_{-\infty}^{\infty} S(Q, E)dE$ is static structure factor given by Fourier transform of the single-time two-point spin correlation function, obtained from DMRG calculations at 200 mK ($\approx 0.01J/k_B$). The temperature dependence of the maximum quantum Fisher information $F_Q(L = 1)$ is shown in Fig. 3D with power-law fits to the asymptotic behavior for both experiment and the idealized DMRG model. Our analysis shows excellent agreement between DMRG and neutron scattering measurements at all temperatures above the magnetic ordering transition, $T_N \approx 0.8$ K. At very low temperatures, F_Q in the idealized model continues to rise, demonstrating at least quadpartite entanglement at 200 mK. In contrast, in $YbAlO_3$ the QFI is arrested with $F_Q \approx 1$ at T_N, though enough spectral weight remains at high energy for it to demonstrate at least bipartite entanglement.

At high-temperature, $F_Q(L = 1)$ exhibits a near-perfect T^{-2} power-law decay for both experiment and theory. Already for temperatures $T \gtrsim 0.5J/k_B$, $F_Q(L = 1)$ is below 1, the value where it indicates the presence of at least bipartite entanglement. Thus F_Q as a metric for quantum coherence has limited usefulness at high temperatures. This poses a challenge of developing novel quantum metrology to capture high-temperature quantum behaviors in integrable systems, including the observed coherence of spinon excitations.

Real-space–time response

The observed long-range dynamical coherence associated with propagating spinons contrasts sharply with the local character of single-time two-spin correlation function, $\langle S_j^z S_{j'}^z \rangle \approx 1/4\delta_{jj'}$ ($\delta_{jj'}$ is Kronecker delta) at $T \gg J/k_B$, and classical expectation of non-propagative, over-damped or diffusive dynamics in this regime[53]. Like QFI, the single-time correlation is insensitive to dynamical coherence because it encodes an energy-integrated (single-time) property, static structure factor,

$S(Q)$. At high temperature, $S(Q) \approx 1/4$ is Q-independent, indicating vanishing single-time spin-spin correlations.

The time-dependent, dynamical correlations revealing spinon coherence can be visualized by Fourier transforming the measured $\chi''(Q, E)$ to describe the real-space linear response, $\chi''(x, t)$[48] (See Supplementary Information for details of data and theoretical analysis and DMRG calculations.). This is shown in Fig. 4 as a sequence of color-plots scaled by the thermal factor T/J, where panels (A–D) show Fourier-transformed (FT) inelastic neutron data, (E–H) show the corresponding Fourier-transforms of our fits to the data, and (I–L) show the space-time theoretical DMRG data. At all temperatures, $\chi''(x, t)$ is measurably nonzero only in a region defined by a coherent "light cone" bounded by the spinon velocity and approaching zero width at the origin ($x \to 0$ as $t \to 0$) in line with purely local single-time correlations. This light cone feature corresponds in the wave-vector-energy domain to the dispersive upper boundary of the spinon spectrum, and its presence at high temperatures testifies to the coherent nature of excitations. Remarkably, the linear ballistic transport regime appears to persist on a mesoscopic length scale at short times even when the thermal energy scale markedly exceeds interactions. At long times, however, the transport appears to cross over into a super-diffusive regime, $x \sim t^{2/3}$. Such a super-diffusive behavior is predicted in the high-temperature limit of the Heisenberg chain and has been of interest for some number of years[54], but to our knowledge this is the clearest experimental signature of such a behavior to date. At very high temperatures, experiment and fits experience a Lorentzian broadening along the energy axis, which indicates a shortening of the coherence time and a faster decay of dynamical correlations absent in the purely theoretical model, Fig. 4(I–L).

Discussion

Topologically-protected spinon excitations in integrable systems present an attractive avenue towards encoding information in the spin degree of freedom in materials. Our work demonstrates remarkable quantum coherent behavior of spinons hosted by the effective $S = 1/2$ Heisenberg chains in $YbAlO_3$, including ballistic propagation at temperatures far exceeding the energy-scales at which individual spins interact with each other. The lifetime of these excitations remains longer than our experimental resolution up to very high temperatures, comparable to the crystal-field levels splitting of the Yb^{3+} ions, whose thermal population destabilizes the ground-state Kramers doublets underlying the spin-1/2 Heisenberg chain physics. In turn, this provides a possible control channel for the quantum-collective behaviors in optically-active rare-earth chains where optically-excited ions can be used to control the propagation of information[16]. Overall, our results suggest that such integrable rare-earth spin-systems may have a far broader range of quantum information applications than previously realized and also challenge quantum metrology to develop new methods suitable for gauging high-temperature dynamical coherence in quantum systems.

Methods

Neutron scattering

The time-of-flight neutron scattering measurements were performed at the Cold Neutron Chopper Spectrometer (CNCS), Spallation Neutron Source (SNS). $E_i = 1.55$ meV ($\lambda = 7.26$ Å) was used. Here, chopper resolution settings resulted in a resolution full-width-half-maximum (FWHM) of 0.038 meV at the elastic position [see also dashed line in Fig. 3A]. A single crystal sample of $YbAlO_3$[21] was mounted with its orthorhombic $\boldsymbol{a}$ direction vertical, which allowed spectral mapping in the $(0, K, L)$ scattering plane. The wave vector, $Q = (H, K, L)$, is measured in reciprocal lattice units of the orthorhombic $Pbnm$ lattice of $YbAlO_3$ ($a = 5.126$ Å, $b = 5.331$ Å, and $c = 7.313$ Å), where Yb-Yb spacing along the chain direction is $d = c/2$. Neutron intensities were binned on a uniform grid in wave-vector and energy, with a focus on two-dimensional slices in the $L - E$ plane. Details of the analyses including fitting to numerical models are described in the Supplementary Information.

Finite-temperature DMRG calculations

The dynamical structure factor (DSF) $S_{\mathrm{DMRG}}(q, E)$ vs. one-dimensional in-chain momentum $q \equiv L/2$ and energy E was computed within DMRG in real-time and real-frequency from the retarded correlation function,

$$S^{\mathrm{ret}}(x, t) \equiv -\mathrm{i}\vartheta(t)\,\langle \hat{S}_x(t)\hat{S}_0^{\dagger}\rangle_T, \tag{3}$$

where $\hat{S}_x(t) \equiv e^{\mathrm{i}\hat{H}t}\hat{S}_x\, e^{-\mathrm{i}\hat{H}t}$ is the spin operator $\hat{S}$ acting on site x at time t in the Heisenberg picture, with $\hat{H}$ the Hamiltonian. Since DMRG operates on a finite system of length $N = 64$ with open boundary conditions (BCs) and lattice constant $d := 1$, the DSF was computed relative to the system center, referred to as origin '0' above, hence having integer $x \in [-N/2 + 1, N/2]$. The time evolution was considered up until the light cone was about to reach the open system boundary. This data was then zero-padded towards larger system $|x| > N/2$ and extended in time via linear prediction, followed by double Fourier transform to momentum q and energy E. Additional details are presented in the Supplementary Information.

Data availability

All data needed to evaluate the conclusions in the paper are present in the paper and the Supplementary Information. Additional data are available from the authors upon request.

References

1. Uhlenbeck, G. E. & Goudsmit, S. Spinning electrons and the structure of spectra. *Nature* **117**, 264 (1926).
2. P. A. M., Dirac*The Principles of Quantum Mechanics*, 4th ed., International series of monographs on physics No. 27 (Clarendon Press, Oxford University Press, Oxford [u.a.], 1930, 4th ed. 1981).
3. Bethe, H. Zur Theorie der Metalle: I. Eigenwerte und Eigenfunktionen der linearen Atomkette. *Z. f.ür. Phys.* **71**, 205 (1931).
4. Tsvelik, A. M. *Quantum Field Theory in Condensed Matter Physics*, 2nd ed. (Cambridge University Press, Cambridge, UK, 2003) title from publisher's bibliographic system (viewed on 05 Oct 2015).
5. Bose, S. Quantum communication through an unmodulated spin chain. *Phys. Rev. Lett.* **91**, 207901 (2003).
6. Venuti, L. C., Boschi, C. D. E. & Roncaglia, M. Qubit teleportation and transfer across antiferromagnetic spin chains. *Phys. Rev. Lett.* **99**, 060401 (2007).
7. Tserkovnyak, Y. & Loss, D. Universal quantum computation with ordered spin-chain networks. *Phys. Rev. A* **84**, 032333 (2011).
8. O. V., Marchukov, A. G., Volosniev, M., Valiente, D., Petrosyan, and N. T., Zinner Quantum spin transistor with a Heisenberg spin chain. *Nature Communications* **7**, https://doi.org/10.1038/ncomms13070 (2016).
9. Thompson, K. F., Gokler, C., Lloyd, S. & Shor, P. W. Time independent universal computing with spin chains: quantum plinko machine. *N. J. Phys.* **18**, 073044 (2016).
10. Kitaev, A. Y. Fault-tolerant quantum computation by anyons. *Ann. Phys.* **303**, 2 (2003).
11. Broholm, C. et al. Quantum spin liquids.*Science* **367**, eaay0668 (2020).
12. Semeghini, G. et al. Probing topological spin liquids on a programmable quantum simulator. *Science* **374**, 1242 (2021).
13. Andrich P., et al. Long-range spin wave mediated control of defect qubits in nanodiamonds. *npj Quantum Information* **3**, https://doi.org/10.1038/s41534-017-0029-z (2017).
14. Lachance-Quirion, D., Tabuchi, Y., Gloppe, A., Usami, K. & Nakamura, Y. Hybrid quantum systems based on magnonics. *Appl. Phys. Express* **12**, 070101 (2019).

15. Chumak, A. V. et al. Advances in magnetics roadmap on spin-wave computing. *IEEE Trans. Magn.* **58**, 1 (2022).
16. Awschalom, D. D., Hanson, R., Wrachtrup, J. & Zhou, B. B. Quantum technologies with optically interfaced solid-state spins. *Nat. Photonics* **12**, 516 (2018).
17. Zhong, T. et al. Nanophotonic rare-earth quantum memory with optically controlled retrieval. *Science* **357**, 1392 (2017).
18. Ruskuc, A., Wu, C.-J., Rochman, J., Choi, J. & Faraon, A. Nuclear spin-wave quantum register for a solid-state qubit. *Nature* **602**, 408 (2022).
19. Beckert, A. et al. Emergence of highly coherent two-level systems in a noisy and dense quantum network.*Nat. Phys.* **20**, 472–478 (2024).
20. Wu, L. S. et al. Antiferromagnetic ordering and dipolar interactions of $YbAlO_3$. *Phys. Rev. B* **99**, 195117 (2019).
21. Wu, L. S. et al. Tomonaga-Luttinger liquid behavior and spinon confinement in $YbAlO_3$. *Nat. Commun.* **10**, 698 (2019).
22. Nikitin, S. E., Xie, T., Podlesnyak, A. & Zaliznyak, I. A. Experimental observation of magnetic dimers in diluted Yb:$YAlO_3$. *Phys. Rev. B* **101**, 245150 (2020).
23. Nikitin S. E., et al. Multiple fermion scattering in the weakly coupled spin-chain compound $YAlO_3$. *Nature Communications* **12**, https://doi.org/10.1038/s41467-021-23585-z (2021).
24. Nichitiu, M. D., Brown, C. & Zaliznyak, I. A. Breakdown of sound in superfluid helium. *Phys. Rev. B* **109**, l060502 (2024).
25. Xu, G. et al. Mesoscopic phase coherence in a quantum spin fluid. *Science* **317**, 1049 (2007).
26. Zaliznyak, I. A., Regnault, L.-P. & Petitgrand, D. Neutron-scattering study of the dynamic spin correlations in $CsNiCl_3$ above Néel ordering. *Phys. Rev. B* **50**, 15824 (1994).
27. Zheludev, A. et al. Extended universal finite-T renormalization of excitations in a class of one-dimensional quantum magnets. *Phys. Rev. Lett.* **100**, 157204 (2008).
28. Sachdev, S. & Damle, K. Low temperature spin diffusion in the one-dimensional quantum O(3) nonlinear σ model. *Phys. Rev. Lett.* **78**, 943 (1997).
29. Huberman, T., Tennant, D. A., Cowley, R. A., Coldea, R. & Frost, C. D. A study of the quantum-classical crossover in the spin dynamics of the 2DS= 5/2 antiferromagnet Rb_2MnF_4: neutron scattering, computer simulations and analytic theories. *J. Stat. Mech.: Theory Exp.* **2008**, P05017 (2008).
30. Bayrakci, S. P. et al. Lifetimes of antiferromagnetic magnons in two and three dimensions: Experiment, theory, and numerics. *Phys. Rev. Lett.* **111**, 017204 (2013).
31. Zaliznyak, I. A. et al. Spinons in the strongly correlated copper oxide chains in $SrCuO_2$. *Phys. Rev. Lett.* **93**, 087202 (2004).
32. Zaliznyak, I. A. A glimpse of a luttinger liquid. *Nat. Mater.* **4**, 273 (2005).
33. Lake, B., Tennant, D. A., Frost, C. D. & Nagler, S. E. Quantum criticality and universal scaling of a quantum antiferromagnet. *Nat. Mater.* **4**, 329 (2005).
34. Mourigal, M. et al. Fractional spinon excitations in the quantum Heisenberg antiferromagnetic chain. *Nat. Phys.* **9**, 435 (2013).
35. Uimin, G., Kudasov, Y., Fulde, P. & Ovchinnikov, A. Low-energy excitations of yb_4as_3 in a magnetic field. *Eur. Phys. J. B* **16**, 241 (2000).
36. Wu, L. S. et al. Orbital-exchange and fractional quantum number excitations in an f-electron metal, Yb_2Pt_2Pb. *Science* **352**, 1206 (2016).
37. Nocera, A., Essler, F. H. L. & Feiguin, A. E. Finite-temperature dynamics of the Mott insulating Hubbard chain. *Phys. Rev. B* **97**, 045146 (2018).
38. Laurell, P. et al. Magnetic excitations, nonclassicality, and quantum wake spin dynamics in the Hubbard chain. *Phys. Rev. B* **106**, 085110 (2022).
39. Zhydachevskyy, Y. et al. Band gap engineering and trap depths of intrinsic point defects in RAlO3 (R = Y, La, Gd, Yb, Lu) perovskites. *J. Phys. Chem. C.* **125**, 26698 (2021).
40. Caux, J.-S. & Hagemans, R. The four-spinon dynamical structure factor of the Heisenberg chain. *J. Stat. Mech.: Theory Exp.* **2006**, P12013 (2006).
41. Gannon, W. J. et al. Spinon confinement and a sharp longitudinal mode in Yb_2Pt_2Pb in magnetic fields. *Nat. Commun.* **10**, 1123 (2019).
42. Faddeev, L. D. & Takhtajan, L. A. What is the spin of a spin wave? *Phys. Lett. A* **85**, 375 (1981).
43. Müller, G., Thomas, H., Beck, H. & Bonner, J. C. Quantum spin dynamics of the antiferromagnetic linear chain in zero and nonzero magnetic field. *Phys. Rev. B* **24**, 1429 (1981).
44. Bougourzi, A. H., Couture, M. & Kacir, M. Exact two-spinon dynamical correlation function of the one-dimensional Heisenberg model. *Phys. Rev. B* **54**, R12669 (1996).
45. Karbach, M., Müller, G., Bougourzi, A. H., Fledderjohann, A. & Mütter, K.-H. Two-spinon dynamic structure factor of the one-dimensional s=1/2 Heisenberg antiferromagnet. *Phys. Rev. B* **55**, 12510 (1997).
46. Caux, J.-S. & Maillet, J. M. Computation of dynamical correlation functions of Heisenberg chains in a magnetic field. *Phys. Rev. Lett.* **95**, 077201 (2005).
47. Caux, J.-S., Konno, H., Sorrell, M. & Weston, R. Tracking the effects of interactions on spinons in gapless Heisenberg chains. *Phys. Rev. Lett.* **106**, 217203 (2011).
48. Scheie A., et al. Quantum wake dynamics in Heisenberg antiferromagnetic chains. *Nature Communications* **13**, https://doi.org/10.1038/s41467-022-33571-8 (2022).
49. Menon, V. et al. Multipartite entanglement in the one-dimensional spin-1/2 Heisenberg antiferromagnet. *Phys. Rev. B* **107**, 054422 (2023).
50. Scheie, A. et al. Witnessing entanglement in quantum magnets using neutron scattering. *Phys. Rev. B* **103**, 224434 (2021).
51. Scheie, A. et al. Erratum: Witnessing entanglement in quantum magnets using neutron scattering [Phys. Rev. B 103, 224434 (2021)]. *Phys. Rev. B* **107**, 059902 (2023).
52. Hauke, P., Heyl, M., Tagliacozzo, L. & Zoller, P. Measuring multipartite entanglement through dynamic susceptibilities. *Nat. Phys.* **12**, 778 (2016).
53. Gennes, P. G. D. Inelastic magnetic scattering of neutrons at high temperatures. *J. Phys. Chem. Solids* **4**, 223 (1958).
54. Bulchandani, V. B., Gopalakrishnan, S. & Ilievski, E. Superdiffusion in spin chains. *J. Stat. Mech.: Theory Exp.* **2021**, 084001 (2021).

Acknowledgments

We are grateful to the SNS staff for invaluable technical assistance and to A. Scheie, C. Broholm, M. Mourigal, and A. Zheludev for valuable discussions. The work at Brookhaven National Laboratory was supported by Office of Basic Energy Sciences (BES), Division of Materials Sciences and Engineering, U.S. Department of Energy (DOE), under contract DE-SC0012704. This research used resources at the Spallation Neutron Source, a DOE Office of Science User Facility operated by Oak Ridge National Laboratory.

Author contributions

I.Z. conceived and directed the study. L.K., I.Z., D.P., A.P., and A.S. carried out neutron scattering experiments and obtained the data. L.K. performed fitting of the neutron spectra. L.K. and I.Z. analyzed the data and prepared the figures. A. W. performed theoretical DMRG calculations. R. K. and A. T. carried out theoretical analyses. L.V. provided the single crystals used in this study. I.Z. and L.K. wrote the paper, with input from all authors.

Competing interests
The authors declare no competing interests.

Additional information
Supplementary information The online version contains supplementary material available at https://doi.org/10.1038/s41467-025-61715-z.

Correspondence and requests for materials should be addressed to Igor A. Zaliznyak.

Peer review information *Nature Communications* thanks the anonymous reviewers for their contribution to the peer review of this work. A peer review file is available.